

Whispering gallery modes in zinc-blende AlN microdisks containing non-polar GaN quantum dots

M. Bürger,^{a)} M. Ruth, S. Declair, J. Förstner, C. Meier, and D. J. As

Department Physik, Universität Paderborn, Warburger Str. 100, 33098 Paderborn, Germany

(Received 9 November 2012; accepted 13 February 2013; published online 26 February 2013)

Whispering gallery modes (WGMs) were observed in 60 nm thin cubic AlN microdisk resonators containing a single layer of non-polar cubic GaN quantum dots. Freestanding microdisks were patterned by means of electron beam lithography and a two step reactive ion etching process. Micro-photoluminescence spectroscopy investigations were performed for optical characterization. We analyzed the mode spacing for disk diameters ranging from 2–4 μm . Numerical investigations using three dimensional finite difference time domain calculations were in good agreement with the experimental data. Whispering gallery modes of the radial orders 1 and 2 were identified by means of simulated mode field distributions. © 2013 American Institute of Physics. [<http://dx.doi.org/10.1063/1.4793653>]

Optical microcavities like semiconductor microdisks offer applications in quantum information technology as well as low threshold lasing devices.^{1,2} Microdisks support strong confined whispering gallery modes (WGMs), which propagate at the disk boundary. Since their introduction many efforts were made to fabricate microdisk lasers with high quality factors (Q-factors) to reduce laser thresholds.³ Compared to other photonic resonators (e.g., photonic crystal nanocavities and nanopillars), the fabrication of microdisks is relatively straight forward and reliable.

In the case of group III-nitrides, only microdisks of wurtzite AlN/InN/GaN have been reported up to now.^{4–6} However, piezoelectric and spontaneous polarization fields in the polar (0001) c-direction of hexagonal GaN induce a quantum confined Stark effect. These built-in electric fields influence the behavior of optoelectronic devices containing quantum dots (QDs) or quantum wells (QWs). The recombination probability of electrons and holes is reduced due to a spatial separation of electron and hole wave functions and limits the performance of photonic devices. Therefore, the fabrication of real non-polar metastable cubic GaN (c-GaN) and AlN (c-AlN) in (001) growth direction is very interesting for future applications.⁷ Accordingly, c-GaN QDs offer a radiative recombination time, which is two orders of magnitude lower compared to wurtzite GaN QDs.^{8,9} Non-polar c-GaN QDs are promising for high repetition rate photonic devices and future devices in quantum information technology. The bases of these devices are highly efficient optical sources. Therefore, QDs can be integrated in optical resonators such as microdisks, which confine light by resonant recirculation.

Recently, zinc-blende AlN epilayers containing c-GaN QDs were synthesized using plasma assisted molecular beam epitaxy (PAMBE).^{10,11} This progress arises possibilities in the fabrication of photonic microcavities to improve the light extraction efficiency of QD emitters. Due to the high chemical

and mechanical stability of GaN and the 3C-SiC substrate structuring of microdisks is a serious challenge. A feasible wet chemical etching technique as for GaAs and Si is not available for epitaxial 3C-SiC.¹² Growth as well as removal of additional sacrificial layers by photoelectrical etching is quite difficult to handle.

In this paper, we demonstrate the integration of non-polar III-V semiconductor quantum emitters in optical microcavities. Specifically, we embedded c-GaN QDs in c-AlN microdisk resonators. The freestanding microdisks located on a 3C-SiC pedestal were fabricated by reactive ion etching (RIE). WGMs were observed in low temperature micro-photoluminescence (μ -PL) measurements and compared to numerical calculations. Modes of different orders were identified by simulations of mode field distributions. Furthermore, the energy separation of the WGMs was analyzed with respect to the microdisk diameter.

Our sample consists of a single layer c-GaN QDs sandwiched between two c-AlN barrier layers. 10 μm 3C-SiC, epitaxially deposited by low-pressure metal organic chemical vapor deposition on top of 500 μm Si (001) was used as a substrate.¹³ At the beginning, a 30 nm c-AlN buffer was grown at 760 °C substrate temperature by molecular beam epitaxy in a Riber 32 MBE system. The growth process was monitored *in-situ* by reflection high energy electron diffraction (RHEED).¹⁴ On top of the c-AlN buffer, one layer of self-assembled c-GaN QDs was deposited by the well known Stranski Krastanov (SK) growth process.¹¹ The QDs were then overgrown by another 30 nm c-AlN layer. The QD densities of uncapped samples measured in former studies by atomic force microscopy are in the order of 10^{11} cm^{-2} .¹⁵ More details about the growth of c-AlN and c-GaN QDs can be found in our previous studies.^{10,16} A schematic sample structure is shown in Fig. 1(a).

Structuring of the microdisks started with the deposition of an 80 nm SiO₂ etching mask deposited by plasma enhanced chemical vapor deposition (PECVD) to minimize the surface and sidewall roughness of the disks. Electron beam lithography was utilized to define microdisks ranging from 2 to 4 μm diameter. Afterwards, circular pillars of 100 nm height were

^{a)} Author to whom correspondence should be addressed. E-mail address: mburger@mail.uni-paderborn.de. Telephone +495251605831. Fax +495251605843.

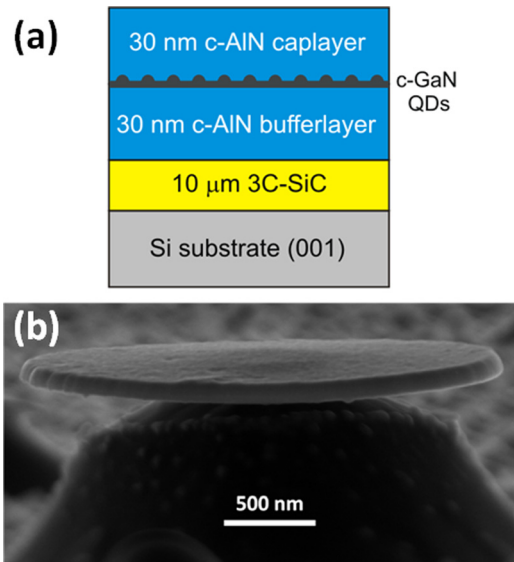


FIG. 1. (a) Schematic structure of a c-AlN microdisk containing c-GaN QDs. (b) Side view SEM image of a 60 nm thick freestanding microdisk with 2.6 μm diameter fabricated by RIE etching.

etched by RIE with SiCl_4 and Ar plasma. Buffered oxide etching solution (BOE) was used to remove the etching mask. The subsequent undercut of the slab was achieved by selective etching of 3 C-SiC using CF_4 RIE at 375 $^\circ\text{C}$ substrate temperature. Fig. 1(b) shows a side view SEM image of a 2.6 μm diameter microdisk. There is no sign of bowing or wrapping of the 60 nm c-AlN slab on the 3 C-SiC pedestal. Slightly vertical striations are visible at the disk edge. Mask erosion during the c-AlN/c-GaN etching step yielded imperfect sidewalls.

A confocal $\mu\text{-PL}$ setup with a 325 nm HeCd laser as excitation source was used for the optical microdisk characterization. The normal incident laser beam is focused by an UV-microscope objective (80 \times , NA = 0.55) and has a diffraction limited spot size ($d \sim 1.22\lambda/\text{NA} \sim 720$ nm). The spectrum was separated by a Czerny-Turner monochromator with a focal length of 0.5 m. The luminescence detection was realized by a UV enhanced charged coupled device (CCD). A piezo controlled sample stage inside a liquid He cryostat enables spatially resolved PL measurements at low temperature.

Analytical solutions for very thin disks exist,¹ however to avoid potential deviations due to the strong approximations involved, numerical calculations were performed with an in-house nonuniform finite-difference time-domain code (FDTD).^{17–19} Mode frequencies and Q-factors were extracted using the Harmonic Inversion method.²⁰ For our geometries, the post of the microdisk had no significant influence on the simulated frequency ladder, most likely due to the small overlap with the modes.

Fig. 2 shows 7 K PL spectra of a non-patterned sample (a) and a microdisk with 2.6 μm diameter (b). The disk diameter was determined by SEM. For clarity, these spectra were shifted upwards. The Gaussian shaped emission band of the reference sample centered at 3.57 eV with a FWHM of 130 meV is related to the QD ensemble luminescence.²¹ The QDs are confined and feature thereby compared to GaN bulk material larger transition energies.²² Due to the high QD density, the emission band is correlated to the size distribution of the QDs.²³ Fabry-Pérot oscillations with a period of

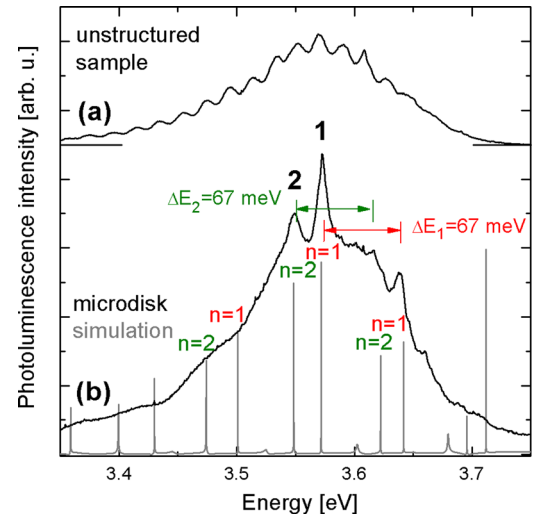


FIG. 2. PL spectra taken at 7 K of an unstructured sample as reference (a) and of c-GaN QDs embedded in a 2.6 μm diameter c-AlN microdisk (black line) compared to FDTD simulations (grey lines) (b). Horizontal arrows indicate the experimental mode spacing of the modes with radial mode orders $n = 1$ and 2.

22 meV originating from the 10 μm thick 3 C-SiC substrate superimpose the reference spectrum.

The PL spectrum (b) of the microdisk (black line) is compared to the calculated mode spectrum of a 2.6 μm microdisk model (grey lines). The emission band located at about 3.58 eV is attributed to the QDs ensemble luminescence again. Since the disk is surrounded by air, there are no 3 C-SiC layer oscillations identifiable. The size distribution of the QDs and a different coupling of the QD emission to the resonator modes cause an inhomogeneously broadened emission peak with a FWHM of 120 meV. If the QD emission couples to resonator modes of the micro cavity, the luminescence intensity increases and additional narrow peaks appear in the QD ensemble spectrum. In the following, we denote the radial mode number n and the azimuthal mode number m . For modes 1 ($E_1 = 3.57$ eV) and 2 ($E_2 = 3.55$ eV), the quality factors ($Q = E/\Delta E$) can be estimated to approximately 600 and 440, respectively. These two resonant modes match well to the calculated resonator modes. The calculated mode spacing of $\Delta E_{1,\text{cal}} = 0.070$ eV ($n = 1$) and $\Delta E_{2,\text{cal}} = 0.072$ eV ($n = 2$) agrees reasonably well with the experimental data of $\Delta E_1 = 0.067$ eV ($n = 1$) and $\Delta E_2 = 0.067$ eV ($n = 2$). Composition fluctuations of the active layer, disk geometry, and the assumption of a constant refractive index during the calculations result in deviations. The assumption of a perfect disk geometry during the calculations results in sharp distinguishable peaks. The mode intensity depends on calculation parameters like the integration time and the excitation pulse.¹⁷

We identified WGMs with Q-factors larger than 400 only around the maximum of the emission peak in the range of 3.55 eV to 3.60 eV. A Gaussian shaped emission band of a QD ensemble is correlated to the size distribution of the QDs. At the maximum of the emission peak, many QDs contribute to the emission band. Therefore, sufficient QD luminescence couple to resonator modes, which results in the appearance of clear WGMs. At both the low and the high energy wing, a significantly smaller fraction of the QD

ensemble contributes to the emission peak. Thus, only a few QDs couple to the resonator modes, which make mode feeding less effective and thus hinders the observation of WGMs. The choice of QDs as the active layer reduces the absorption losses $Q_{\text{abs}}^{-1} \approx \frac{\alpha \lambda}{2\pi n_{\text{eff}}}$ compared to QWs.^{6,24} Since our samples consist of only a single QD layer, it can safely be assumed that the reabsorption is lower than, e.g., in QW samples. Therefore, we suggest light scattering at the sidewalls and the top and bottom surfaces of the microdisk as the main loss mechanism, which is limiting the Q-factors.²⁵

For advanced investigations of the resonator modes 1 and 2, FDTD simulations of WGM field profiles were carried out. Fig. 3 shows the calculated H_z field distributions of modes 1 and 2. We attribute mode 1 in Fig. 3(a) to a WGM with a radial order of $n=1$ and an azimuthal mode number of $m=34$. A second order WGM, like mode 2 (Fig. 3(b)), is propagating closer to the absorbing 3 C-SiC post at the disk center, which usually leads to lower luminescence intensities and Q-factors. The azimuthal mode number of mode 2 is $m=29$.

Fig. 4 shows PL spectra taken at 7 K of different microdisks with 2, 3, and 4 μm diameter. We observe clear WGMs for each microdisk at different emission energies. The energy separation between two modes with the same radial order is indicated by horizontal arrows and decreases from 93 meV (2 μm microdisk) to 48 meV (4 μm microdisk). Calculated mode spectra are plotted again for each microdisk. The calculated mode spacing agrees with our PL results, which supports our interpretation of the additional emission peaks as WGMs. Next to the radial modes of $n=1$ with high intensities, several modes with lower intensities are apparent, which belong to second and third order radial modes. Especially, in case of the 4 μm microdisk, many additional higher order modes occur. The mode types were identified on the basis of calculated field distributions of WGMs as shown in Fig. 3. The estimation for the resonator mode at $E=3.645$ eV of the 4 μm microdisk exhibits a Q-factor of 1400. Comparable WGMs in hexagonal AlN microdisks with 2 μm diameter incorporating hexagonal GaN QDs showed a Q-factor up to 5000.²⁶ However, these hexagonal microdisks were grown on Si (111) substrates, where the Si under-etching could be performed by a selected wet chemical etch, which usually produces smoother sidewalls and a smoother bottom surfaces of the microdisk structure. Scattering at imperfections of the surfaces and sidewall of the disk as well as absorption processes influence the propagating electromagnetic wave at the disk periphery. In our case, we expect that further enhancement of the Q-factors

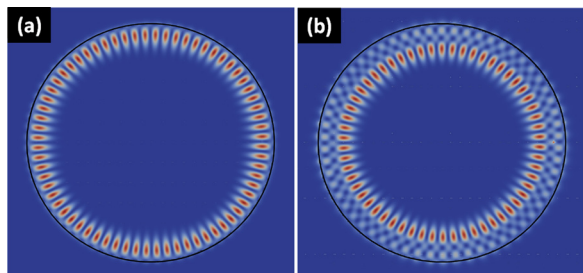


FIG. 3. (a) FDTD simulations of the WGM at $E_1=3.57$ eV (mode 1, $n=1$) and (b) of the WGM at $E_2=3.55$ eV (mode 2, $n=2$). The black circle illustrates the edge of the 2.6 μm microdisk. Red corresponds to the highest and blue to the lowest field density.

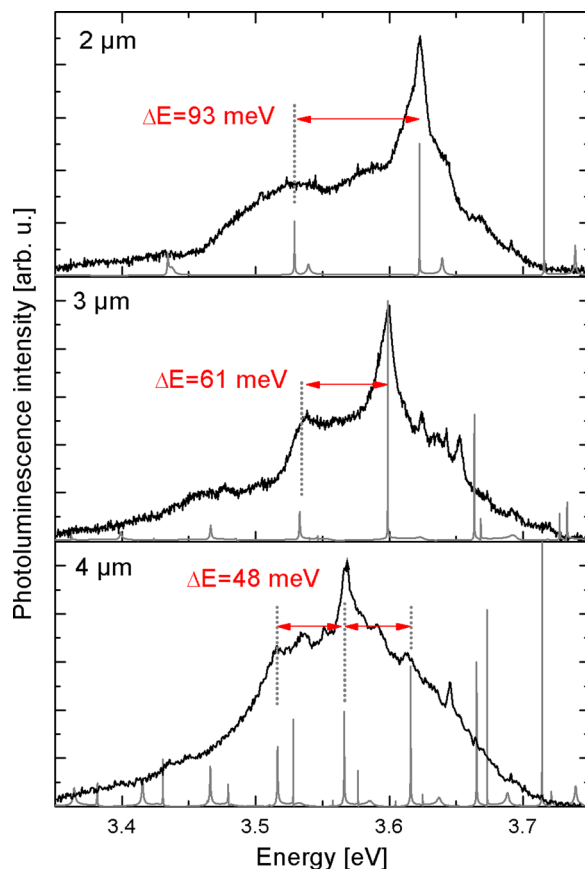


FIG. 4. PL spectra taken at 7 K of microdisks with different diameters (black lines). FDTD calculations (grey lines) are plotted to identify resonator modes. The mode spacing (indicated by horizontal arrows) increases with decreasing disk diameter.

could be achieved by improving the microdisk cavity, as optimized etch parameters may lead to smoother disk sidewalls and surfaces and thereby to lower scattering probability.

Fig. 5 shows the energy separation of the resonator modes as a function of the microdisk diameter. We measured the disk diameters in SEM studies with an accuracy of 100 nm and estimate the error of the experimental mode spacing to 10%. The calculated values of the numerical calculations (triangles) match very well to the experimental

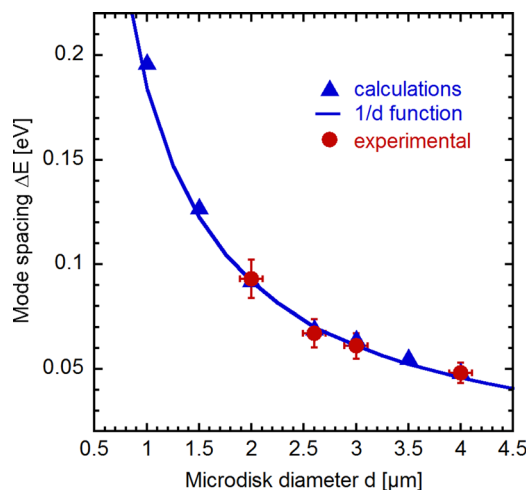


FIG. 5. Correlation between mode spacing and the microdisk diameter. The experimental results are indicated by dots and the mode spacing of the FDTD calculations by triangles. The fitted graph shows $1/d$ dependence of our data.

data (dots). The typical inversely proportional dependence of both results is illustrated by the fitted graph using $\Delta E \approx \frac{\hbar c_0}{R n_{\text{eff}}}$, where c_0 is the free space wavelength, R the disk radius, and n_{eff} the effective refractive index.²⁷

We have fabricated undercut mushroom shaped microdisks of metastable non-polar cubic group III-nitrides. The active layer consists of a single layer non-polar c-GaN QDs symmetrically sandwiched between two 30 nm thick c-AlN confinement layers. Our disks were patterned by electron beam lithography and etched by two sequenced dry etching steps. Micro-photoluminescence measurements at low temperature exhibit the appearance of WGMs with Q-factors exceeding 1400. The dependence of the mode spacing as a function of the disk diameter was investigated. The PL spectra are in good agreement with the calculated mode spectra obtained by three dimensional FDTD simulations. Furthermore, we identified WGMs of different radial orders using simulations of mode field distributions.

This work was supported by the DFG graduate Program GRK 1464 “Micro and Nanostructures in Optoelectronics and Photonics.” K. Lischka is acknowledged for helpful discussions.

¹S. L. McCall, A. F. J. Levi, R. E. Slusher, S. J. Pearton, and R. A. Logan, *Appl. Phys. Lett.* **60**, 289 (1992).

²K. J. Vahala, *Nature* **424**, 839 (2003).

³A. Pawlis, M. Panfilova, D. J. As, K. Lischka, K. Sanaka, T. D. Ladd, and Y. Yamamoto, *Phys. Rev. B* **77**, 153304 (2008).

⁴E. D. Haberer, R. Sharma, C. Meier, A. R. Stonas, S. Nakamura, S. P. DenBaars, and E. L. Hu, *Appl. Phys. Lett.* **85**, 5179 (2004).

⁵A. C. Tamboli, E. D. Haberer, R. Sharma, K. H. Lee, S. Nakamura, and E. L. Hu, *Nat. Photonics* **1**, 61 (2007).

⁶D. Simeonov, E. Feltin, A. Altoukhov, A. Castiglia, J.-F. Carlin, R. Butté, and N. Grandjean, *Appl. Phys. Lett.* **92**, 171102 (2008).

⁷D. J. As, *Microelectron. J.* **40**, 204 (2009).

⁸J. Simon, N. T. Pelekanos, C. Adelman, E. Martinez-Guerrero, R. André, B. Daudin, L. S. Dang, and H. Mariette, *Phys. Rev. B* **68**, 035312 (2003).

⁹T. Bretagnon, P. Lefebvre, P. Valvin, R. Bardoux, T. Guillet, T. Taliercio, and B. Gil, *Phys. Rev. B* **73**, 113304 (2006).

¹⁰T. Schupp, K. Lischka, and D. J. As, *J. Cryst. Growth* **312**, 3235 (2010).

¹¹T. Schupp, T. Meisch, B. Neuschl, M. Feneberg, K. Thonke, K. Lischka, and D. J. As, *AIP Conf. Proc.* **1292**, 165 (2010).

¹²D. Zhuang and J. H. Edgar, *Mater. Sci. Eng. R* **48**, 1–46 (2005).

¹³T. Chassagne, A. Leycuras, C. Balloud, P. Arcade, H. Peyre, and S. Juillaguet, *Mater. Sci. Forum* **457–460**, 265 (2004).

¹⁴J. Schörmann, S. Potthast, D. J. As, and K. Lischka, *Appl. Phys. Lett.* **90**, 041918 (2007).

¹⁵M. Bürger, T. Schupp, K. Lischka, and D. J. As, *Phys. Status Solidi C* **9**(5), 1273 (2012).

¹⁶T. Schupp, K. Lischka, and D. J. As, *J. Cryst. Growth* **312**, 1500 (2010).

¹⁷S. Declair, C. Meier, T. Meier, and J. Förstner, *Photonics Nanostruct. Fundam. Appl.* **8**, 273 (2010).

¹⁸A. Taflove and S. Hagness, *Computational Electrodynamics: The Finite-Difference Time-Domain Method* (Arthouse Tech, Boston, 2005).

¹⁹A. Farjadpour, D. Roundy, A. Rodriguez, M. Ibanescu, P. Bermel, J. D. Joannopoulos, S. G. Johnson, and G. Burr, *Opt. Lett.* **31**, 2972 (2006).

²⁰V. A. Mandelshtam and H. S. Taylor, *J. Chem. Phys.* **107**, 6756 (1997).

²¹T. Schupp, K. Lischka, and D. J. As, *J. Cryst. Growth* **323**, 286 (2011).

²²D. J. As, F. Schmilgus, C. Wang, B. Schöttker, D. Schikora, and K. Lischka, *Appl. Phys. Lett.* **70**, 1311 (1997).

²³G. Schmid, *Nanoparticles: From Theory to Application* (Wiley-VCH, New York, 2006).

²⁴R. E. Slusher, A. F. J. Levi, U. Mohideen, S. L. McCall, S. J. Pearton, and R. A. Logan, *Appl. Phys. Lett.* **63**, 1310 (1993).

²⁵S. Sergent, J. C. Moreno, E. Frayssinet, Y. Laaroussi, S. Chenot, J. Renard, D. Sam-Giao, B. Gayral, D. Néel, and S. David, *J. Phys.: Conf. Ser.* **210**, 012005 (2010).

²⁶M. Mexis, S. Sergent, T. Guillet, C. Brimont, T. Bretagnon, B. Gil, F. Semond, M. Leroux, D. Néel, S. David, X. Chécoury, and P. Boucaud, *Opt. Lett.* **36**, 2203 (2011).

²⁷M. K. Chin, D. Y. Chu, and S. T. Ho, *J. Appl. Phys.* **75**, 3302 (1994).